Water Research 278 (2025) 123324

Contents lists available at ScienceDirect

Water Research

journal homepage: www.elsevier.com/locate/watres

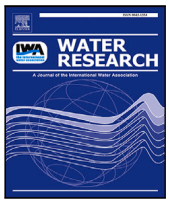

Unveiling the adsorption mechanism of perfluorooctane sulfonate onto polypropylene nanoplastics: A combined theoretical and experimental investigation

Federica Simonetti [a], Marco Mancini [b], Valentina Gioia [b], Rosaceleste Zumpano [a], Franco Mazzei [a], Alessandro Frugis [b], Valentina Migliorati [c,*]

[a] Department of Chemistry and Drug Technologies, Sapienza University of Rome, P.le Aldo Moro 5, 00185, Rome, Italy
[b] Department of Organic Micropollutants, Acea Infrastructure, Via Vitorchiano 165, 00189, Rome, Italy
[c] Department of Chemistry, Sapienza University of Rome, P.le Aldo Moro 5, 00185, Rome, Italy

ARTICLE INFO

Keywords:
PFAS
Sensor
Nanoplastic
Drinking water
Adsorption mechanism

ABSTRACT

Polypropylene (PP) is a key component of nanoplastics detected globally in water, which can carry pollutants through co-transport. In this regard, the co-transport of perfluoroalkyl substances (PFAS) by nanoplastics (NPs) raises significant concern, as NPs can act as vectors that enhance PFAS uptake and bioaccumulation in organisms during co-exposure. In this context, research has shown interactions between NPs and PFAS, but the adsorption mechanism remains still unclear. In this work, a powerful synergic approach combining several computational and experimental techniques has been used to unveil the adsorption mechanism of perfluorooctanesulfonate (PFOS), which is one of the most widespread contaminants of emerging concerns (CECs) on PP nanoparticles. According to our DFT results, PFOS adsorbs onto the outer and inner surface of the nanoparticle, with a maximum adsorption energy of ≈ 18 kcal/mol and an adsorption mechanism mainly governed by dispersion forces between the two fragments. Batch experiments have confirmed that PFOS rapidly adsorbs on PP nanoparticle, showing that pH can reduce the adsorption capacity thus affecting the co-transport. Moreover, the dipole moment of the PFOS-nanoparticle complex has been found to be significantly larger as compared to the bare nanoparticle, resulting in a more pronounced transport in aqueous environment and making the PFOS-PP nanoparticle complex much more dangerous than the bare PP nanoparticle. Altogether, our results allowed us to disentangle the adsorption mechanism of PFAS on PP nanoparticles, which is a fundamental step to understand the co-occurrence of such dangerous pollutants in environmental matrices, as well as to obtain new information for toxicity and risk-models development.

1. Introduction

According to statistics, 1 in 4 people in the world still lacks access to safely managed drinking water (Ritchie et al., 2019). To exacerbate the situation is the occurrence of contaminants of emerging concerns (CECs) in soil and aquatic ecosystems, that along with their environmental and toxicological impacts, degrade water quality standards and pose a significant risk to both the environment and population worldwide (Sandoval et al., 2024). CECs encompass several classes of compounds, such as perfluoroalkyl substances (PFAS), pharmaceuticals and personal care products, pesticides and plastics, which may have an even more detrimental impact on human health than other well-known common contaminants (Pizzini et al., 2024; M.D. Hernando et al., 2006). Among them, plastics and PFAS stand out due to the concern they are raising within the scientific community and global consciousness. Each year, 19–23 million metric tonnes of mismanaged plastic waste are discharged in water basins (Borrelle et al., 2020; Bergmann et al., 2022), and thus, despite limitations, plastics waste are often detected in the environment (Koelmans et al., 2019). To give an idea, while it takes just few milliseconds to decide to throw a small plastic bottle into the sea, it will take over 450 years to degrade. During this extremely slow degradation process, due to weathering and biotic interactions (Bergmann et al., 2022; Enfrin et al., 2019), the bottle breaks down into smaller pieces called meso-plastics, i.e. small plastics fragments with size of 5–40 mm (Peng et al., 2020), which further fragments into micro-plastics (MPs, plastic particles in the range of 1-5000 μm), and nano-plastics (NPs, i.e. plastic particles in the range of 1 to 1000 nm) (Gigault et al., 2018; Pelegrini et al., 2023). Nevertheless,

* Corresponding author.
E-mail address: valentina.migliorati@uniroma1.it (V. Migliorati).

https://doi.org/10.1016/j.watres.2025.123324
Received 5 November 2024; Received in revised form 10 January 2025; Accepted 17 February 2025
Available online 25 February 2025

the toxicological effects of micro- and nano-plastics (MNPs) on the human health have not been well established (Haldar et al., 2023; Pelegrini et al., 2023). NPs are thought to be more dangerous than MPs, due to their smaller size that is associated to a higher reactivity, stronger interactions with microorganism (Yee et al., 2021) and their ability to be internalized and penetrate into biological tissues (Llorca and Farré, 2021). Moreover, they are very abundant, their significant burden in the ecosystem being due to the weathering of plastic litters and fragments. The ability of NPs to work as enhanced adsorbers/vectors of other legacy contaminants (Rai et al., 2022; Agboola and Benson, 2021; Qi and Qin, 2024), pathogens (Sun et al., 2023) and CECs (Tseng et al., 2022; Liu et al., 2019), such as PFAS (Salawu et al., 2024), has a huge impact on the planetary public health. The sorption mechanism of such substances on NPs is regulated by many factors, like NPs size, shape, and surface chemistry and, due to this mechanism, the adsorbed contaminants may be released in remote areas, causing bio-accumulation and magnification in the aquatic environment (Cara et al., 2022; Jeong et al., 2018; Wang et al., 2019). As well as MNPs, PFAS are persistent organic pollutants (POPs), so widely dispersed in water matrices that their contamination represents a planetary boundary that is going to be exceeded (Cousins et al., 2022; Kurwadkar et al., 2022). Perfluorooctanoic acid (PFOA) and perfluorooctane sulfonate (PFOS) are the most detected PFAS in environmental matrices and they have been associated with plastic pollution (Wee and Aris, 2023; Joo et al., 2021) and endocrine dysfunction (Fenton et al., 2021; Wee and Aris, 2017; Podder et al., 2021; Deep and Ahluwalia, 2001). Adsorption kinetic and biotoxicity studies investigated the co-occurrence of PFAS and NPs, finding that PFOS and PFOA are the most adsorbed PFAS onto environmental MNPs (Cheng et al., 2021; Navarathna et al., 2023; Chen et al., 2023). A recent study demonstrated that the adsorption of PFAS onto secondary polyethylene terephthalate (PET) MPs in water is thermodynamically spontaneous, with equilibrium reached within a 7–9 h timeframe and higher adsorption observed for perfluorosulfonic acids, primarily due to their high degree of hydrophobicity (Salawu et al., 2024). In addition, it was demonstrated that the gastrointestinal fluids in organisms may promote the desorption of PFAS from MPs, thus augmenting the hazard (Bakir et al., 2014; Liu et al., 2020). Despite the significant impact that the co-transport of these compounds by NPs may have on living organisms, most studies have primarily focused on the experimental investigation of PFAS adsorption onto MPs, with very few studies examining the adsorption onto NPs, especially from a mechanistic perspective (Christian et al., 2022; Minervino and Belfield, 2024; Townsend, 2024; Liu et al., 2023a; Cortés-Arriagada, 2021). Even if the sorption mechanism is believed to be primarily driven by hydrophobic interactions (Salawu et al., 2024; Zenobio et al., 2022; Ateia et al., 2020; Wang et al., 2015; Llorca et al., 2018), other forces may play a role and become important at the nanoscale, highlighting the need to fully elucidate their co-transport and combined toxicity in ecosystems. The aim of this paper is to shed light, at an atomistic level, into the co-transport of PFAS and nanoparticles. In particular, we have investigated the sorption of PFOS, which is one of the most widespread compounds in water matrices, onto NPs made of polypropylene (PP), a polymer widely used during the Cov-19 pandemic for face masks (Zhao et al., 2024) and that is, along with PET, globally detected (Koelmans et al., 2019). In a previous work we had shown that PFAS are adsorbed on PP containers, Mancini et al. (2023) and we expect that such adsorption is even enhanced in PP nanoparticles, due to their very high adsorption ability associated with their large surface to volume ratio. To investigate the co-transport mechanism, we have used a powerful approach which combines theoretical calculations based on density functional theory (DFT) and experimental data to obtain quantitative information on the adsorption process. This synergic study aims to contribute to a better understanding of the interfacial process at molecular scale and of the role of nanoplastics in the co-transport, bioaccumulation and bioavailability of PFAS in the ecosystems.

2. Experimental

2.1. Chemicals and reagents

PP pellets (MW = 12 kDa), xylene and ethanol were purchased at the highest purity available from Sigma-Aldrich (St. Louis, MO, USA). Optima LC-MS grade acetonitrile (ACN), ultrapurewater, and methanol (MeOH) were purchased from Biosolve (Valkenswaard, Netherlands). LC-MS grade (>99%) ammonium acetate (CH_3COONH_4) was purchased from VWR International Srl (Pennsylvania, USA). Vials (Phenomenex, part.no.AR0-3611-12) were purchased from Phenomenex (Torrance, USA). Thermo Scientific$_{TM}$ Nalgene$_{TM}$ Rapid-Flow$_{TM}$ sterile Disposable Filter Units with Nylon membranes (0.2 μm pore size, $P/N164-0020$) were purchased from Thermo Fisher Scientific (Waltham, United States) and tested before the usage to avoid PFAS contamination. Analytical standards including PFOS technical solution and mass labeled standard ($^{13}C_4$ PFOS) were purchased from Wellington Laboratories (1,2 mL, 50 μg/mL in methanol)(Guelph, ON, Canada), kept away from PFAS packaging and material during storage. Calibration solutions, with concentrations of 1–1000 ng/L, were prepared by serial dilutions of the stock solution in 30:70 (v/v) methanol/water.

2.2. Methods

2.2.1. PP nanoparticles synthetic protocol

PP nanoparticles were synthesized through the solvent–antisolvent precipitation method following a previous established protocol (Lee et al., 2022), with some modifications. Briefly, 30 mg of PP pellets were dissolved into 3 g of xylene and heated at 110 °C until no visible traces of PP remained. Once heating was stopped, 15 mL of hot ethanol was added to the solution, leading to the formation of a white precipitate. The suspension was stirred for 2 h until it cooled down, and the precipitate was collected by vacuum filtration using a pre-tested 0.2 μm Nylon membrane filter and dried at 80 °C overnight to remove any residual solvent.

2.2.2. Characterization of PP nanoparticles

Morphology and shape were investigated using High-Resolution Field Emission Scanning Electron Microscopy (HR FESEM, Zeiss Auriga Microscopy). The PP nanoparticles suspension in ethanol was dropped onto a GaAs wafer and allowed to dry. After drying, a 10 μm layer of chromium was sputter-coated onto the sample. The size distribution of the PP nanoparticles from the FESEM images was evaluated using the ImageJ software. The specific surface area (S_e) of the PP nanoparticle has been calculated by using the following equation:

$$S_e = \frac{6}{\rho} D_s \quad (1)$$

where ρ is the bulk density and D_s is the Sauter mean diameter.

2.3. Instrumental analysis

The UHPLC-MS/MS system employed in this study comprised a Thermo Scientific UHPLC UltiMate 3000 system fitted with a Thermo Scientific TSQ Altis triple quadrupole mass spectrometer equipped with a ESI ionization probe. The chromatographic separation of the compounds was performed on a Luna Omega PS C18 (Phenomenex, $P/N00D-4752-AN$) analytical column (100 × 2.1 mm, 1.6 μm particles sizes), with a security C18 Luna (Phenomenex, $P/N00A-4252-Y0$) guard column (5 μm, 100 Å, 30 × 3 mm), while the mass spectra were recorded in negative ion mode. The total run time was 15 min with a flow rate of 0.3 mL/min and a gradient mode developed in our study, using water acidified with 5 mM ammonium acetate (A) and ACN (B) as mobile phases. The time program started with 98% eluent A for 0.5 min, then eluent A decreased to 70% over 0.1 min. From 0.6 to 8 min, eluent A was further decreased to 0% and held constant for 1 min. After that, eluent A was raised to 98% in 0.1 min

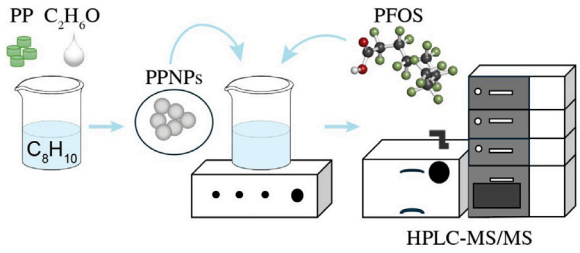

Fig. 1. Schematic representation of the PP nanoparticles synthesis and batch adsorption experiments.

and held at 98% until the end of the gradient (15 min). The column temperature was 313 K, the internal autosampler temperature was set at 298 K and the injection volume was 100 μL. The mass spectrometer parameters in negative ionization mode were as follows: spray voltage of −2.5 kV, sheath gas flow rate of 50 a.u., auxiliary gas flow rate of 10 a.u., sweep gas flow rate of 1 a.u., while the ion transfer tube was at 598 K and the vaporizer at 573 K. MS/MS analysis was run in the multiple reaction monitoring (MRM) mode. For native and mass-labeled PFOS quantification, the monitored mass transitions are 499–80 (Collision Energy, CE, of 47 V) and 503–80 (CE of 40 V), respectively. The adopted protocol is shown in Fig. 1.

2.4. PFOS adsorption studies

The adsorption of PFOS onto PP nanoparticles was studied by a batch method at room temperature (298 ± 2 K) under controlled settings (Brandani, 2021), by adding known amount of PP nanoparticles (10 mg) to a 5 mL PFOS solution (500 ng/L) in amber glass vials. The concentrations of PFOS and PP nanoparticles were selected to achieve an optimal compromise between environmental background levels and reaction kinetics. Temperature was continuously monitored and maintained constant throughout the experiment, and the samples periodically collected at 0, 45, 90, 150, 240, 300 and 600 min. At the end of the adsorption experiments, 700 μL aliquots were transferred to LC glass vials. Then, the aliquots were spiked with 0.1 ng of the mass-labeled internal standard (50 μg/L) and diluted to 1 cc with methanol for LC-MS/MS analysis, as described in Section 2.1. Both pH and conductivity were measured before and after the addition of the adsorbent and adsorbate, as well as at the conclusion of the batch adsorption experiments. As preliminary tests to assess the effect of aqueous chemistry, we investigated the influence of pH and ionic strength based on literature-reported ranges, typical of engineered and natural aquatic systems (Zhang et al., 2012; Essien et al., 2008; Satpathy et al., 2010; Klungness and Byrne, 2000; P. Cervantes-Avilás et al., 2017). The initial pH was adjusted to the desired values (5, 7, or 9) using 0.1 M NaOH or HCl, while the effect of salinity was assessed by varying the NaCl concentration (0.1 M). To ensure high confidence in the data, all experiments were performed in triplicates, with triplicate controls. These measurements included calibrators, blank samples, quality control samples, and method validation. Multiple blank samples were run after each analysis to ensure that there was no contamination from the LC-MS/MS system or reagents. The kinetics were also conducted in the absence of PP nanoparticles to assess the potential partitioning of PFOS onto the container walls. The response of the analyte was recorded as the ratio between the peak area of the native standard and the peak area of the mass-labeled internal standard. The adsorption capacity (ng/g) at specific time t q_t and at equilibrium q_{eq} were calculated using the equations below:

$$q_t = \frac{(C_i - C_t) * V}{M} \tag{2}$$

$$q_{eq} = \frac{(C_i - C_{eq}) * V}{M} \tag{3}$$

where C_i, C_t, and C_{eq} are the initial concentration and the concentration of the adsorbate at time t and at equilibrium, respectively. V is the volume of the solution (L) and M is the mass of the adsorbent (g).

2.5. Quantum mechanical calculation details

A combination of Quantum Mechanical (QM) methods and theoretical procedures of analysis was employed to investigate the adsorption of PFOS on PP nanoparticles, along the line of previous studies (Liu et al., 2023b; Cortés-Arriagada et al., 2023a). A model of PP nanoparticles containing 224 atoms was constructed starting from an PP polymer chain consisting of 24 units (C_3H_6), with a molecular weight of 1.038 kDa, by using the Gabedit program (Allouche, 2011). NPs in nature have rough and amorphous structures (Hildebrandt and Thünemann, 2023). Therefore, 500 ps MD simulations at 500 K in the canonical ensemble were carried out to fold single polymer chains, followed by a conformational search using the AMBER force field parameters (Allouche, 2011). In this context, the spherical shape was chosen as the target because several experimental studies have found that a sphere is the preferred shape of NPs in water (Gigault et al., 2018). Moreover, it is easily standardized and can be used as a reference shape for comparison with other studies (Tanaka et al., 2021). The resulting NP has a surface area of 1331 A^2 (with a diameter of 2.0 nm), which is relatively larger than that of the selected compound (591 A^2), ensuring good coverage properties and a reasonable compromise between computational cost and accuracy. QM calculations have been carried out by means of the Orca4.2.1 package (Neese, 2018), using DFT. Full geometry optimizations were performed using the PBE functional (Perdew et al., 1996) and the all-electron def2-SVP basis set (Weigend and Ahlrichs, 2005). The energies and all of the other properties have then been calculated using the hybrid B3LYP functional (Becke, 1993). Solvent effects have been implicitly included in the calculations by using the CPCM formalism, Barone and Cossi (1998) with water as solvent ($\epsilon = 80.4$). Dispersion force corrections were also included with the DFT-D3 method, together with the Becke-Johnson damping function (Grimme et al., 2011). Note that solvent effects and dispersion force corrections have been included in the calculations of all of the properties described below and in the single point energy calculations, but not in the geometry optimizations due to the high computational cost of such calculations.

The stability of the PFOS-PP nanoparticle (PFOS-PPNP) complexes have then been evaluated by calculating the adsorption energies E_{ads}:

$$E_{ads} = E_{PFOS} + E_{PPNP} - E_{PFOS\text{-}PPNP} \tag{4}$$

where $E_{PFOS\text{-}PPNP}$ is the energy of the adsorption complex, E_{PFOS} is the isolated PFOS energy and E_{PPNP} is the isolated PP nanoparticle energy. According to Eq. (4), the more positive the E_{ads} value, the more stable the PFOS-PPNP complex. Energy decomposition analysis based on absolutely localized molecular orbitals with implicit solvent (water) model, ALMO-EDA(solv) (Khaliullin et al., 2007, 2008) was used to determine the nature of the interaction between the adsorbate and the NP. Such approach decomposes the adsorption energy into six physical contributions:

$$-E_{ads} = E_{ELEC} + E_{DISP} + E_{POL} + E_{CT} + E_{PAULI} + E_{PREP} \tag{5}$$

where E_{ELEC}, E_{DISP}, E_{POL}, and E_{CT} are the stabilizing energies due to classical intermolecular electrostatic, dispersion forces, polarization and charge transfer effects, respectively, while E_{PAULI} is the destabilizing energy due to steric Pauli repulsion. E_{PREP} is the destabilizing preparation energy due to geometric/electronic distorsion of each fragment. The ALMO-EDA(solv) calculations were carried out using the Q-Chem software (Shao et al., 2015) at the B3LYP-D3/def2-SVP level of theory. Wavefunction, fragmental charge population, and molecular dipole moment analyses were performed by means of Multiwfn 3.8 (Lu and Chen, 2012). Note that the dipole moments have been calculated by setting the origin of coordinates to the center of nuclear charges.

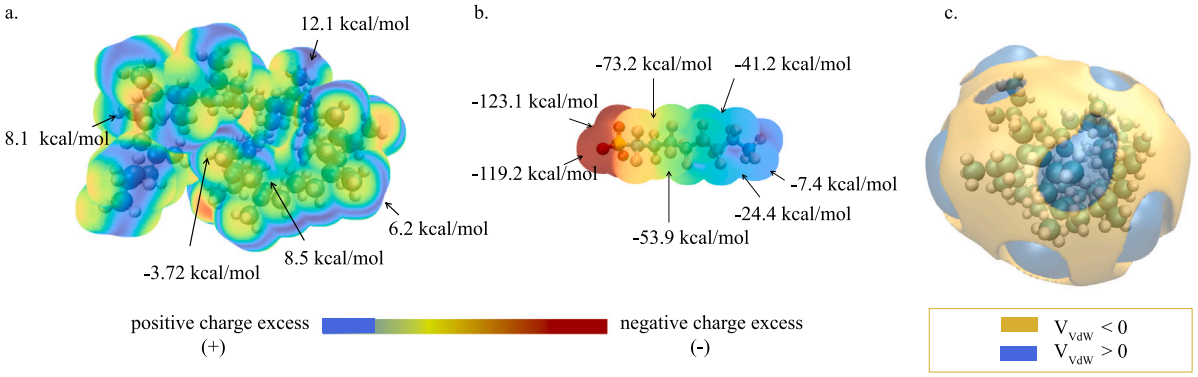

Fig. 2. Electrostatic potential (ESP) map of PP nanoparticles (a) and PFOS (b). Selected maximum and the minimum values of the ESP on the molecular surfaces (ρ = 0.001 a.u.) are also shown. (c) V_{vdW} surface around the PP nanoparticles. Blue and yellow colors represent regions where V_{vdW} is positive and negative, respectively. (For interpretation of the references to color in this figure legend, the reader is referred to the web version of this article.)

In addition to electrostatic potential (ESP) analysis, Van der Waals potential (V_{vdW}) analysis was also carried out to highlight regions where dispersion forces allow the formation of stabilizing interactions with the adsorbate (Lu and Chen, 2020). In such analysis, V_{vdW} is written as the sum of two terms:

$$V_{vdW} = V_{repul} + V_{disp} \quad (6)$$

where V_{repul} and V_{disp} are the repulsion and dispersion potentials, respectively. The nature of intermolecular interactions was visualized using the Independent Gradient Model based on Hirshfeld partitioning (IGMH), implemented in the main function 20 (visual study of weak interaction) of Multiwfn, as described by Lu and Chen (2022). The IGMH can portray covalent and non-covalent interactions counterparts in two intra- and intermolecular regions (Rayene et al., 2022) expressed as follow:

$$\delta g = \delta g_{intra} + \delta g_{inter} \quad (7)$$

where δg_{intra} and δg_{inter} indicate intramolecular and intermolecular contributions to the gradient of electron density, respectively. This method was employed to calculate the three-dimensional real space function δg_{inter} and the color-filled maps of δg_{inter} was drawn via the VMD code in order to highlight the different interactions.

3. Results and discussion

3.1. Surface properties and adsorption energies

To gain insight into the adsorption mechanism, the nature of the interactions between PFOS and the PP nanoparticle was thoroughly investigated. The ESP maps of PFOS and PP nanoparticle are shown in Fig. 2a and b, where red and blue zones represent the negative (electron-rich) and positive (electron-deficient) charged regions, respectively. The ESP maps can predict nucleophilic and electrophilic sites, providing insights into the interaction behavior of a molecular system. PP is a non-polar molecule, constituted by C and H atoms. The slight difference in electronegativity between H and C [2.20 (H) and 2.55 (C) in the Pauling scale] causes partial charges that account for the positive and negative sites observed in the map. The small ESP values (≈−4 to +12 kcal/mol) in Fig. 2a indicate the presence of a weak surface charge, which is predominantly positive (80%), and corresponds to a very weak surface polarity of ≈ 0.4 Debye (*vide infra*). On the opposite site, PFOS is an eight-carbon compound featuring an oleophobic perfluorinated alkyl chain and a hydrophilic head, which allows it to act as a surfactant. The acidic sulfonic head group is predominantly dissociated in most environmental and biological compartments (pKa < 1), while the fluoro-substituted chain contributes

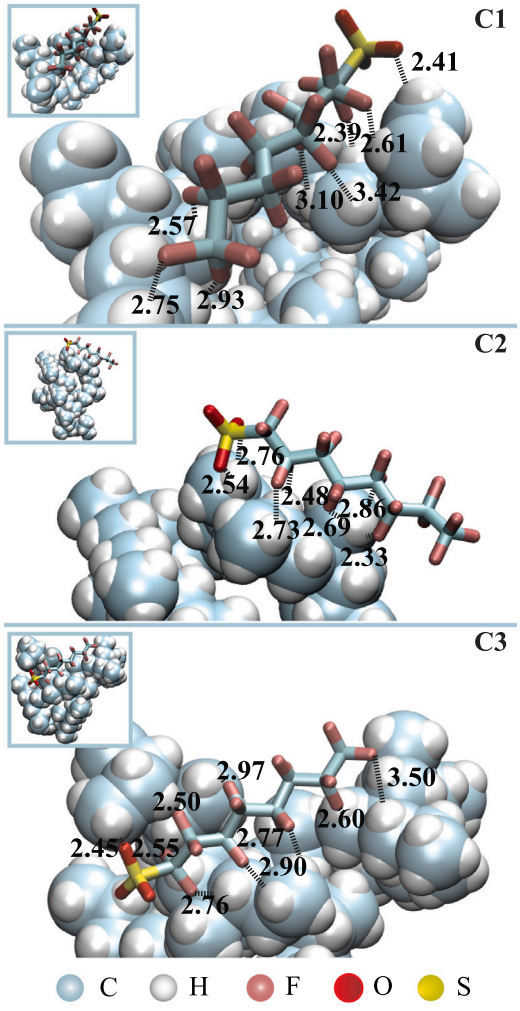

Fig. 3. Molecular structures of the PFOS-PPNPs complexes C1, C2 and C3. Representative intermolecular distances between the PFOS F atoms and the nanoparticle H atoms (Å) are indicated with black numbers. (For interpretation of the references to color in this figure legend, the reader is referred to the web version of this article.)

to hydrophobic interactions and is unfavorable for interactions with water, facilitating sorption onto hydrophobic sorbent materials (Rayne and Forest, 2009; Pontius, 2019; He et al., 2024). Additionally, the negatively charged head group may engage electrostatic interactions

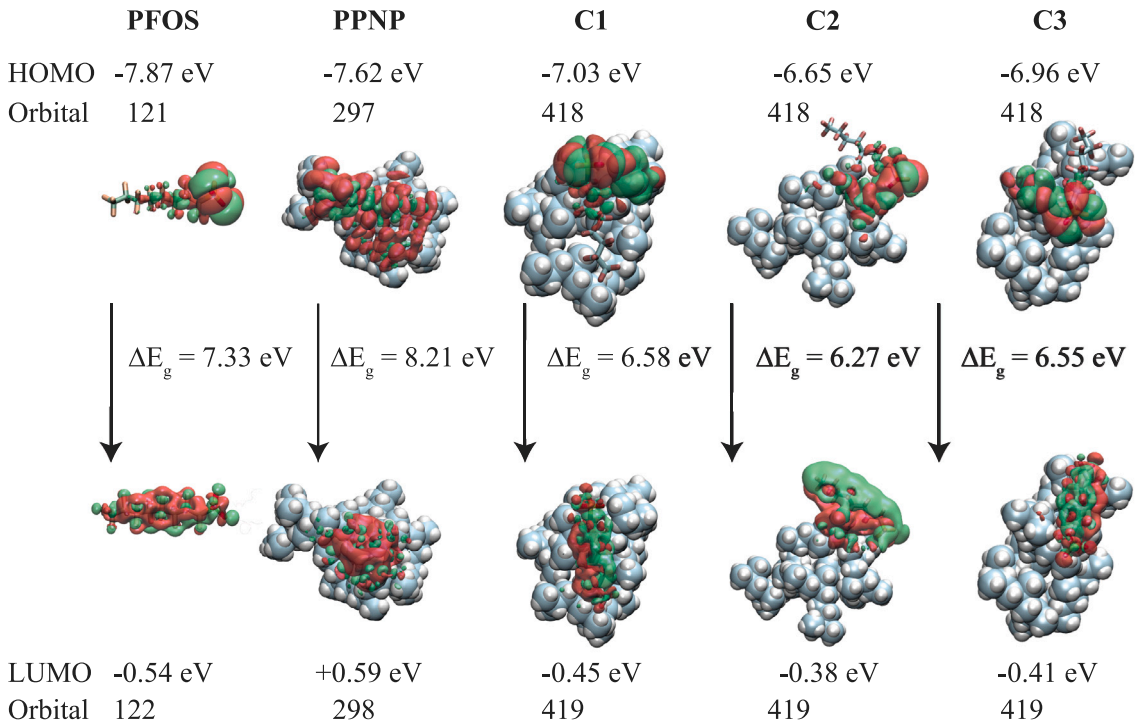

Fig. 4. Distribution of the HOMO and LUMO of the PFOS and the PP nanoparticle fragments before the adsorption process and of their complexes C1, C2 and C3. The energies of each orbital and the HOMO-LUMO energy gap (ΔE_g) are also shown.

with particles with opposite charge. The ESP map of PFOS clearly highlights these regions in red, indicating its potential for non-covalent electrostatic interactions with the positively charged regions of the PP nanoparticle. Therefore, PP nanoparticles can adsorb PFAS through Coulombic attractions.

Besides such electrostatic interactions, dispersion forces are expected to play a crucial role in the interaction mechanism. In order to investigate the surface properties of PP nanoparticles and visualize the regions susceptible to contaminant physisorption, the V_{vdW} was analyzed and mapped (see Fig. 2c). The large yellow regions stands for the negative part of V_{vdW} and represent the regions where attractive dispersion effects will surpass exchange repulsion effects. Therefore, in such PP nanoparticle regions adsorbate molecules can be adsorbed via dispersion forces. In order to shed light on the mechanism for PFOS sorption on PP nanoparticles, we have carried out ab initio optimizations of PFOS-PPNP complexes, as described in the Methods section. Among all of the simulated configurations, the three PFOS-PPNP most representative structures are shown in the insets of Fig. 3, labeled as C1, C2 and C3. In all the configurations, non-covalent interactions are formed, with bond lengths ranging between 2.33 and 3.50 Å. Fig. 3 shows the intermolecular distances that are found in the three complexes. In particular, all the shortest distances between the F atoms of the PFOS anion and the H atoms of the nanoparticle have been reported, within a cutoff distance value of 3.50 Å.

Several studies suggest that co-transport of contaminants can occur on both the outer and inner surfaces of polymeric nanoparticles. Due to its highly polar head group, PFOS is likely to adsorb on the surface of PP nanoparticles (Liu et al., 2018a). On the other hand, it has been observed experimentally that small PFAS molecules can partially diffuse into the material's pores (Salawu et al., 2024). In our three most representative structures, PFOS exhibits both inner and outer adsorption on PP nanoparticles. The most stable configuration is C1, corresponding to an inner adsorption, with an adsorption energy of 18.3 kcal/mol and shorter bond distances, as compared to the other structures, that can be compatible with the formation of polar interactions, as observed in other PFAS systems (Leung et al., 2023). The C2 configuration exhibits an outer adsorption, while C3 a partial inner adsorption, with adsorption energies of 10.5 and 14.0 kcal/mol, respectively. The positive adsorption energy values obtained in all cases indicate the formation of stable complexes in water environment. Moreover, they are comparable with the energies previously found for other adsorbates on several NPs (see Table 1). Our results show that in the adsorption process of PFOS on PP nanoparticles an inner adsorption is the preferred mechanism, suggesting that the formation of stabilizing interactions in this case dominates the repulsion effects.

Additional insights into the adsorption process has been gained by calculating the frontier molecular orbitals of the system. In the frontier molecular orbital theory, the highest occupied molecular orbital (HOMO) is referred to the occupied orbital with the highest energy, the lowest unoccupied molecular orbital (LUMO) is referred to the empty orbital with the lowest energy, and HOMO and LUMO orbitals are generally called frontier orbitals. According to such theory, the closer the energy of HOMO and LUMO orbitals of two interacting fragments, the stronger the interaction and the greater the degree of stability of the system. The distribution of the HOMO and LUMO of the PFOS and the PP nanoparticle fragments before the adsorption process and of their complexes is shown in Fig. 4. The LUMO of PFOS is broadly distributed from the sulfonic head group to the fluorine atoms near the carbon chain, while the HOMO is more localized around the sulfonic head. On the other hand, the HOMO and LUMO of the PP nanoparticle are widely spread across its surface, even if the LUMO tend to be less widespread. After the adsorption process, in all the configurations C1, C2 and C3 the HOMO orbitals of the complexes are predominantly distributed around the sulfonic head group of PFOS, resembling the distribution found in the HOMO of PFOS, but the orbital spreads to some extent also to the atoms of the nanoparticle that are located near the adsorbate polar head. On the contrary, the LUMO orbital of the three complexes spread across the entire PFOS anions, as well as on the nearest nanoparticle atoms. By calculating the HOMO-LUMO energy gap (ΔE_g) of the three configurations, that are reported in Fig. 4, it is interesting to observe that the trend obtained resembles the trend of the adsorption energies

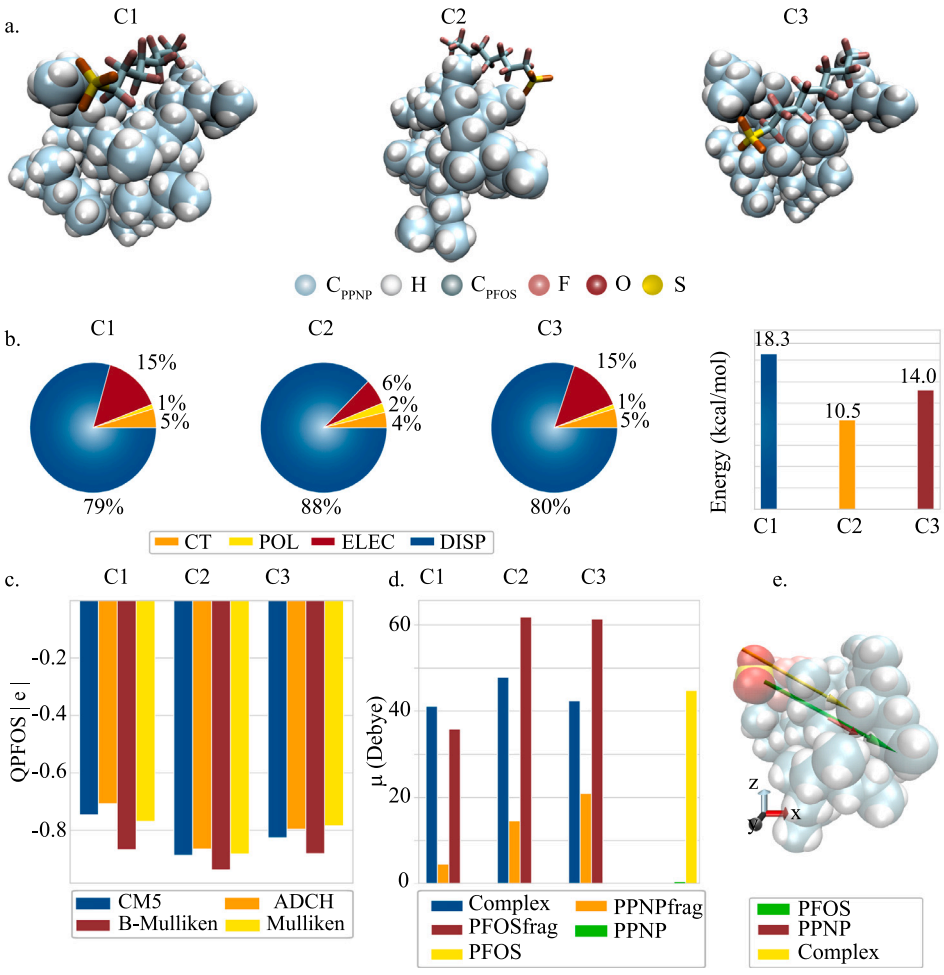

Fig. 5. A. Molecular structures of the PFOS-PPNPs complexes C1, C2 and C3. b. Relative single percentage contributions of ALMO-EDA(solv) energies and adsorption energies (E_{ads}) values for the three complexes C1, C2 and C3. c. Fragmental charge of PFOS calculated using different methods (left panel) and dipole moment analysis (right panel) for the complex, the isolated PFOS and PP nanoparticles and the fragmental dipole of PFOS and PP nanoparticles in the complex. d. Dipole moment vectors for the complex C1, and the fragmental dipoles of PFOS and PP nanoparticles in the complex (x-z plane).

Table 1
Comparison of adsorption energies E_{ads} (kcal/mol) for several molecules and adsorbents.

Molecule	Adsorbent	Method	E_{ads} (kcal/mol)	Ref.
Bisphenol A	PETNPs	DFT/B3LYP	19.3	Cortés-Arriagada (2021)
Diclofenac	PSNPs	DFT/B3LYP	14.9	Cortés-Arriagada et al. (2023a)
Caffeine	PSNPs	DFT/B3LYP	14.1	Cortés-Arriagada et al. (2023a)
PFOS	PEMPs	MD	102.3	Enyoh et al. (2022)
PFOS	PP	DFT	5.5	Zenobio et al. (2022)
PFOS	PPNPs	DFT/B3LYP	18.3	This work

(C1 > C3 > C2). This result indicates that the configurations that are more stable in terms of interaction energies, are also more stable from an electronic point of view.

3.2. Adsorption mechanism

In order to explore the specific role of the stabilizing effects involved in the interactions formed between PFOS and the PP nanoparticle, we have decomposed the adsorption energy of each configuration C1, C2 and C3 (shown for reference in Fig. 5a) by using the ALMO-EDA(solv) approach. Destabilizing effects in the complexes are mainly due to Pauli repulsion, while the geometric preparation contribution due to adsorption is negligible in all cases. Such destabilization is overcompensated by the stabilizing driving forces, especially the dispersion ones, resulting in a favorable adsorption process and positive adsorption energies in all the complexes. In particular, dispersion forces account for the 79%–88% of stabilization, followed by electrostatic interactions (6%–15%), charge transfer (4%–5%) and polarization effects (1%–2%), in minor contributions (see Fig. 5b). The contribution of E_{POL} is very low for all the configurations, and this can be in part due to the fact that polarization is diminished by solvent screening effects. Note that both E_{CT} and E_{POL} contributions are short-range terms, that decay approximately exponentially along with the intermolecular distances. In general, adsorption processes can be accompanied by electron transfer, bonds formation/disruption and geometry rearrangements, in such a way that chemical and physical adsorption are sometimes intertwined (Liu et al., 2018b). In our case, even if PFOS adsorption on the PP nanoparticle is mainly driven by non-covalent interactions, a weak amount of intermolecular electron transfer takes place, giving rise to a charge rearrangement in the complexes and to a change of polarity. In order to evaluate the charge transfer that takes places in the complexes, the PFOS fragmental charge has been calculated as index

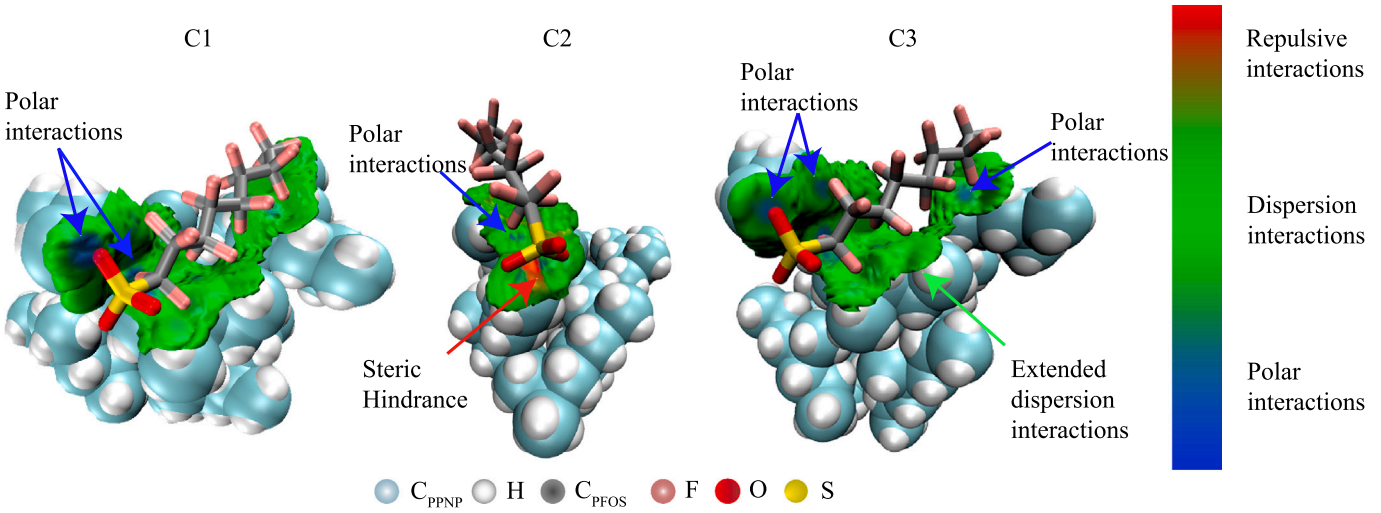

Fig. 6. Independent gradient model based on Hirshfeld partitioning (IGMH) analysis of non-covalent intermolecular interactions taking place in the PFOS-PP complexes C1, C2 and C3. (For interpretation of the references to color in this figure legend, the reader is referred to the web version of this article.)

of electron transfer. Four different population analysis were considered for comparison and the results of this analysis are shown in the left panel of Fig. 5c. Taking the average value calculated using the different analysis for each complexes, a charge transfer of 0.23, 0.11 and 0.18 |e| was observed between PFOS and the PP nanoparticle for the C1, C2 and C3 clusters, respectively. The electron transfer is in the direction of the PP nanoparticle, due to the electrophilic nature of the nanoparticle surface. Interestingly, in agreement with the frontier molecular orbital analysis, the highest value of electron transfer obtained is related to the C1 complex which is the more stable one. Moreover, it is important to stress that such charge transfer may activate the C–H groups of PP, favoring C–H–O and C–H–F interactions (Enyoh et al., 2022; Cortés-Arriagada et al., 2023b; Dalvit et al., 2014). We have then calculated the dipole moment of each complex, isolated fragments and the fragmental dipoles of the PFOS and nanoparticle fragments in the complex (see Fig. 5c). The pollutant dipole moment remains high even after complexation, favoring an high dipole moment of the entire complex. It is clearly observable that the dipole moment of the PP nanoparticle, which is almost zero in the isolated molecule, significantly increases after complexation, due to the alignment of dipole moments post-complexation. To provide a visual insight, Fig. 5d shows the fragmental and complex dipoles in the C1 configuration as arrows. Since the dipole moment vectors of the fragments favorably align along the x and z axes, the dipole moment of the complex is larger compared to the fragmental dipoles. It is noteworthy that the complex dipole moment is much larger than that of the free nanoparticle which is almost zero, contributing to a more pronounced transport in aqueous environments. This behavior make the PP nanoparticle with the adsorbed PFOS much more dangerous than the bare nanoparticle: the increased transport in aqueous media indeed increases the exposition and hence the probability to end up in drinking water. Finally, the intermolecular interactions were explored by the Independent Gradient Model based on Hirshfeld partition (IGMH) (Lu and Chen, 2022). Fig. 6 shows the isosurface of the δg_{inter} function. The blue and green colors highlight the regions where polar interactions and dispersion forces occur. The dispersion interactions are the dominant forces that take place in all the complexes, in agreement with the ALMO-EDA(solv) results, with additional contributions from polar interactions between the oxygen atoms of the polar head and the fluorine atoms of the PFOS hydrophobic chain and the hydrogen atoms of the nanoparticle moiety. The polar interactions are shown by small blue elliptic δg_{inter} spots that are particularly visible in the C1 complex.

The red isosurfaces represent regions where steric destabilization takes place due to repulsive interactions between PFOS and the PP nanoparticle. As it can be seen, only in the C2 configuration there is a small repulsive region, showing that the complex experiences a certain amount of steric hindrance. Altogether these results show that the stability of the PFOS-PPNP complexes is governed by the formations of favorable dispersive interactions between PFOS and the PP nanoparticle, with additional contributions of electrostatic interactions and polar interactions. Therefore, our findings allowed us to shed light on the relative contributions of driving forces in the process of adsorption of PFOS on PP nanoparticles, in order to establish a consensus on the interaction mechanisms between these pollutants.

3.3. Adsorption experiments

To support quantum mechanical calculations, batch adsorptions experiments have been carried out, as detailed in Methods section. To this end, PP nanoparticles have been synthesized using a modified non-solvent induced protocol (Lee et al., 2022). This methodology allowed for the rapid, surfactant-free production of uniform-distributed sphere-like PP nanoparticles with a high yield (80%), as shown in Fig. 7a. The average diameter of the PP nanoparticles was of 619 ± 191 nm (n = 200), as obtained from their size distribution shown in Fig. 7b. The morphological analysis revealed that the surface of PPNP is rough with pores with a mean size of 3 ± 2 nm, which may allow contaminants inner adsorption. Note that the pore size distribution has been analyzed starting from the SEM measurements by means of the ImageJ code. Moreover, we have calculated the specific surface area by using Eq. (1) and we have obtained a S_e value of 6.79 m^2/g. Such value is of the same order of magnitude but larger than that recently obtained by means of the Brunauer–Emmett–Teller (BET) measurements for secondary PET microplastics (Salawu et al., 2024). It is important to stress that the S_e value obtained has to be considered an estimate, since it does not take into account the porosity of the nanoparticles.

The PP nanoparticles are well dispersible in aqueous matrices, being suitable for adsorption experiments. The colloidal stability of the nanoparticle dispersion is demonstrated by their low ζ potential (−58.53 ± 1.76 mV) in deionized water (Lee et al., 2022), mainly due to the adsorbed hydroxide ions (Hildebrandt and Thünemann, 2023; Cassano et al., 2021). In the single-analyte solution, PFOS was rapidly adsorbed and the equilibrium was reached in 240 min (see Fig. 7c), significantly earlier than the microplastics (420 min, Salawu et al. (2024)). Moreover, as it can be seen in the figure, the partitioning of

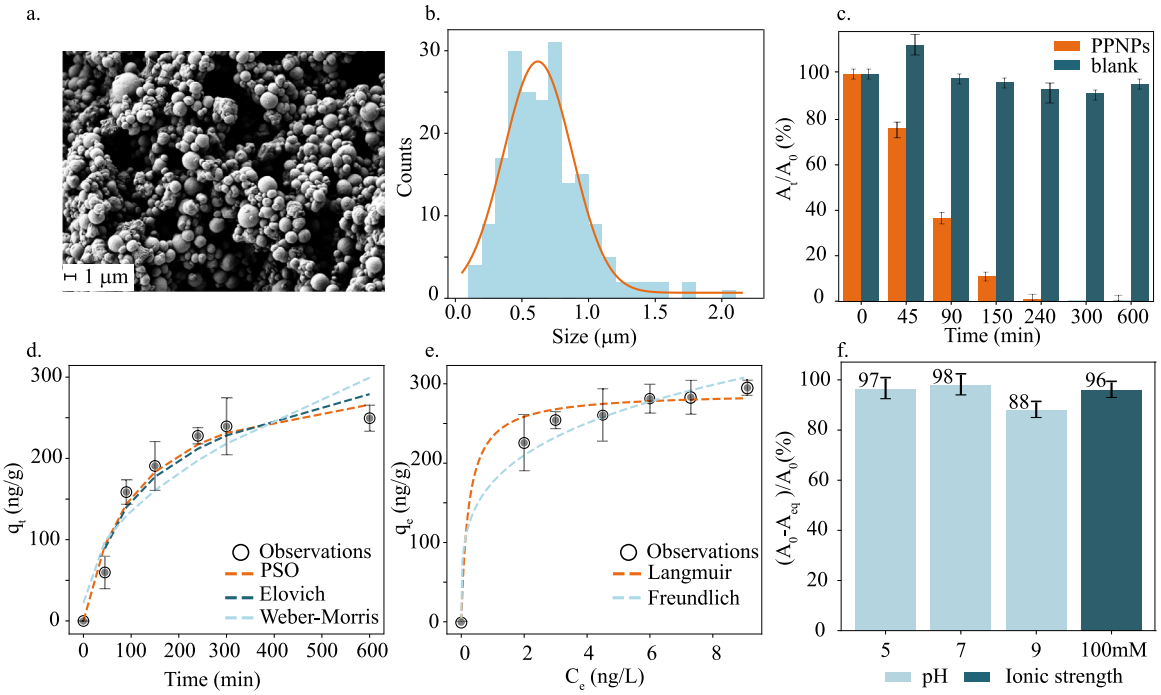

Fig. 7. Batch adsorption results. (a and b) SEM image of PP nanoparticles and their size distribution; (c) Percentage of mass signal decrease in the absence and presence of 2 g/L of PP nanoparticles (pH = 7, deionized water, [PFOS] = 500 ng/L); (d) Non-linear kinetic fitting results (Pseudo-Second Order - PSO, Elovich, and Weber-Morris models); (e) Adsorption isotherm curves (Langmuir and Freundlich non-linear fitting) performed in deionized water at room temperature (298 ± 2 K) using the equilibrium time determined for PFOS in the presence of 2 g/L of PP nanoparticles. The range of PFOS initial concentrations tested was between 450 and 600 ng/L; (f) Equilibrium sorption percentage at different pH (5,7,9) and ionic strength (100 mM).

PFOS onto the glass container (blank sample) is not competitive within the adsorption timeframe, in agreement with the results reported in our previous work (Mancini et al., 2023). As observable in Fig. 7d, the kinetic of PFOS adsorption onto PP nanoparticles is best described by the second-order model (PSO) (q_{eq} = 312.99 ± 29.04, K_2 = 30.18 ± 10.84 g mg^{-1} min^{-1}, R^2 = 0.96), while also the Elovich and Weber and Morris models are suitable (Vareda, 2023). These models were chosen because they are widely used to describe adsorption processes in liquid media (Salawu et al., 2024; Liu et al., 2019). The fitting results confirm that the adsorption mechanism is primarily driven by dispersion interactions, while diffusion into particle pores or surfactant self-aggregation may represent the rate-limiting steps (Plazinski et al., 2013). However, the latter plays a minor role considering the low working concentration range with respect to the CMC. To gain further insight into the adsorption mechanism, we also conducted adsorption isotherm experiments (Fig. 7e). In such experiments, we have considered the equilibrium time determined from the kinetic study. Both the Langmuir and Freundlich models fit the data well: the best fit of the Langmuir model (q_{max} = 316.6 ± 5.9 (ng/g), K_L = 1.25 ± 0.15 (L/ng), R^2 = 0.996) suggests that PFOS adsorption is monolayer and that there are no interactions between PFOS anions. Moreover, the calculated equilibrium parameter (R_L = 0.6) suggests that the adsorption is favorable. The good fit of the Freundlich model (R^2 = 0.960), on the other hand, is not surprising given the system's heterogeneity. Altogether these experimental results are in line with our computational findings and confirm that PFOS rapidly adsorbs on PP nanoparticles and that dispersion forces are the main interaction forces driving the adsorption mechanism. In addition, the equilibrium sorption capacity was evaluated as percentage at different pH (5, 7, and 9) and ionic strength conditions (100 mM). pH could play a role in the adsorption mechanism by either reducing or enhancing the adsorption capacity of the PP nanoparticles. As shown in Fig. 7f, a pH ≥ 9 could decrease the adsorption capacity, likely due to the adsorption of hydroxide ions onto the PP nanoparticles surface through electrostatic interactions. On the other hand, the effect of a ionic strength of 100 mM (and pH = 7), which corresponds to the salts concentration in seawater, has been evaluated (Fig. 7f). The obtained result shows that the ionic strength does not affect the adsorption process under the specific conditions we used. However, it is important to stress that it could have an effect in different conditions.

4. Conclusions

In this work, for the first time the adsorption mechanism of PFOS on PP nanoparticles has been elucidated using a powerful synergic approach which combines several computational and experimental techniques. DFT calculations have shown that PFOS adsorbs onto the outer and inner surface of PP nanoparticles, with a maximum adsorption energy of ≈ 18 kcal/mol. The adsorption mechanism is mainly driven by the establishment of dispersion forces between the two fragments, with electrostatic and H-bonds interactions giving a minor contribution to the complex stabilization. Batch experiments have confirmed that PFOS rapidly absorbs onto the PP nanoparticles, demonstrating that pH can reduce the adsorption capacity by affecting the co-transport. Besides the concerning adsorption properties of PP nanoparticles with respect to the investigated pollutant, an additional alarming aspect that emerges from this study is that when PFOS adsorbs on the nanoparticles, the dipole moment of the aggregate increases significantly compared to the bare nanoparticle, resulting in a more pronounced transport in aqueous environment and making the PFOS-PPNP complex much more dangerous than the bare PP nanoparticle. Altogether our results allowed us to disentangle the adsorption mechanism of PFAS on PP nanoparticles, which is fundamental to design efficient water treatment methods to eliminate such dangerous pollutants, as well as to obtain new information for toxicity studies and risk-models development. This study represents a first step towards a profound understanding of the complex mechanisms taking place in real aquatic systems. The theoretical calculations and the experiments carried out in this work have been performed on an ideal system consisting solely of water and the adsorption complex. Future work should

focus on investigating, both theoretically and experimentally, real environmental conditions present in aqueous basins to better capture the complexities and variability of actual systems. In this framework, from a theoretical point of view, a powerful tool to proceed further would be carrying out molecular dynamics simulations of systems that mimic environmental conditions, such as the presence of natural organic matter or the possibility to have a multicomponent scenario instead of a single PFAS adsorbed on the nanoplastic.

CRediT authorship contribution statement

Federica Simonetti: Writing – review & editing, Writing – original draft, Visualization, Software, Methodology, Data curation, Conceptualization. **Marco Mancini:** Methodology, Investigation, Conceptualization. **Valentina Gioia:** Methodology, Investigation. **Rosaceleste Zumpano:** Methodology, Investigation. **Franco Mazzei:** Validation, Resources. **Alessandro Frugis:** Validation, Supervision, Resources, Conceptualization. **Valentina Migliorati:** Writing – review & editing, Supervision, Software, Methodology, Data curation, Conceptualization.

Declaration of competing interest

The authors declare that they have no known competing financial interests or personal relationships that could have appeared to influence the work reported in this paper.

Acknowledgments

The authors would like to acknowledge the facilities and resources provided by ACEA Infrastructure S.p.A.. The authors are also grateful for the support of the National Center for Water Safety (CeNSIA) of the Italian National Institute of Health (ISS). Finally, the authors wish to extend their thanks to Dr. Gianluca Zanellatto of SNNLab (Sapienza University) for his helpful advice on various technical issues examined in this paper and to Dr. Stefano Brillarelli for his invaluable contributions to the graphics.

Data availability

Data will be made available on request.

References

Agboola, O., Benson, N., 2021. Physisorption and chemisorption mechanisms influencing micro (nano) plastics-organic chemical contaminants interactions: A review. Front. Env. Sci. 9, 678574.

Allouche, A.R., 2011. Gabedit—a graphical user interface for computational chemistry softwares. J. Comput. Chem. 32, 174–182.

Ateia, M., Zheng, T., Calace, S., Tharayil, N., Pilla, S., Karanfil, T., 2020. Sorption behavior of real microplastics (mps): insights for organic micropollutants adsorption on a large set of well-characterized mps. Sci. Total. Env. 720, 137634.

Bakir, A., Rowland, S.J., Thompson, R.C., 2014. Enhanced desorption of persistent organic pollutants from microplastics under simulated physiological conditions. Environ. Pollut. 185, 16–23.

Barone, V., Cossi, M., 1998. Quantum calculation of molecular energies and energy gradients in solution by a conductor solvent model. J. Phys. Chem. A 102, 1995–2001.

Becke, A.D., 1993. A new mixing of hartree–fock and local density-functional theories. J. Chem. Phys. 98, 1372–1377.

Bergmann, M., Collard, F., Fabres, J., Gabrielsen, G.W., Provencher, J.F., Rochman, C.M., van Sebille, E., Tekman, M.B., 2022. Plastic pollution in the arctic. Nat. Rev. Earth Env. 3, 323–337.

Borrelle, S.B., Ringma, J., Law, K.L., Monnahan, C., Lebreton, L., McGivern, A., Murphy, E., Jambeck, J., Leonard, G.H., Hilleary, M.A., Eriksen, M., Possingham, H.P., Frond, H.D., Gerber, L.R., Polidoro, B., Tahir, A., Bernard, M., Mallos, N., Barnes, M., Rochman, C.M., 2020. Predicted growth in plastic waste exceeds efforts to mitigate plastic pollution. Science 369, 1515–1518.

Brandani, S., 2021. Kinetics of liquid phase batch adsorption experiments. Adsorption 27, 353–368.

Cara, B., Lies, T., Thimo, G., Robin, L., Lieven, B., 2022. Bioaccumulation and trophic transfer of perfluorinated alkyl substances (pfas) in marine biota from the belgian north sea: Distribution and human health risk implications. Environ. Pollut. 311, 119907.

Cassano, D., La Spina, R., Ponti, J., Bianchi, I., Gilliland, D., 2021. Inorganic species-doped polypropylene nanoparticles for multifunctional detection. ACS Appl. Nano Mater. 4, 1551–1557.

Chen, X., Qadeer, A., Liu, M., Deng, L., Zhou, P., Mwizerwa, I.T., Liu, S., Ajmal, Z., Xingru, Z., Jiang, X., 2023. Chapter 13 - bioaccumulation of emerging contaminants in aquatic biota: Pfas as a case study. In: Kumar, M., Mohapatra, S., Weber, K. (Eds.), Emerging Aquatic Contaminants. pp. 347–374.

Cheng, Y., Mai, L., Lu, X., Li, Z., Guo, Y., Chen, D., Wang, F., 2021. Occurrence and abundance of poly-and perfluoroalkyl substances (pfass) on microplastics (mps) in pearl river estuary (pre) region: Spatial and temporal variations. Environ. Pollut. 281, 117025.

Christian, E.E., Qingyue, W., Weiqian, W., Tanzin, C., Mominul, H.R., Rezwanul, I., Guo, Y., Lin, Y., Kai, X., 2022. Sorption of per- and polyfluoroalkyl substances (pfas) using polyethylene (pe) microplastics as adsorbent: Grand canonical monte carlo and molecular dynamics (gcmc-md) studies. J. Env. Anal. Chem. 0, 1–17.

Cortés-Arriagada, D., 2021. Elucidating the co-transport of bisphenol a with polyethylene terephthalate (pet) nanoplastics: A theoretical study of the adsorption mechanism. Environ. Pollut. 270, 116192.

Cortés-Arriagada, D., Miranda-Rojas, S., Camarada, M.B., Ortega, D.E., Alarcón-Palacio, V.B., 2023a. The interaction mechanism of polystyrene microplastics with pharmaceuticals and personal care products. Sci. Total. Env. 861, 160632.

Cortés-Arriagada, D., Ortega, D.E., Miranda-Rojas, S., 2023b. Mechanistic insights into the adsorption of endocrine disruptors onto polystyrene microplastics in water. Environ. Pollut. 319, 121017.

Cousins, I.T., Johansson, J.H., Salter, M.E., Sha, B., Scheringer, M., 2022. Outside the safe operating space of a new planetary boundary for per- and polyfluoroalkyl substances (pfas). Res. J. Env. Toxicol. 56, 11172–11179.

Dalvit, C., Invernizzi, C., Vulpetti, A., 2014. Fluorine as a hydrogen-bond acceptor: Experimental evidence and computational calculations. Chem. - Eur. J. 20, 11058–11068.

Deep, S., Ahluwalia, J.C., 2001. Interaction of bovine serum albumin with anionic surfactants. Phys. Chem. Chem. Phys. 3, 4583–4591.

Enfrin, M., Dumée, L.F., Lee, J., 2019. Nano/microplastics in water and wastewater treatment processes – origin, impact and potential solutions. Water Res. 161, 621–638.

Enyoh, C.E., Wang, Q., Wang, W., Chowdhury, T., Rabin, M.H., Islam, R., Yue, G., Yichun, L., Xiao, K., 2022. Sorption of per-and polyfluoroalkyl substances (pfas) using polyethylene (pe) microplastics as adsorbent: Grand canonical monte carlo and molecular dynamics (gcmc-md) studies. J. Env. Anal. Chem. 104, 1–17.

Essien, J., Benson, N., Antai, S., 2008. Seasonal dynamics of physicochemical properties and heavy metal burdens in mangrove sediments and surface water of the brackish qua iboe estuary, nigeria. Toxicol. Env. Chem. 90, 259–273.

Fenton, S.E., Ducatman, A., Boobis, A., DeWitt, J.C., Lau, C., Ng, C., Smith, J.S., Roberts, S.M., 2021. Per-and polyfluoroalkyl substance toxicity and human health review: Current state of knowledge and strategies for informing future research. Environ. Toxicol. Chem. 40, 606–630.

Gigault, J., ter Halle, A., Baudrimont, M., Pascal, P.Y., Gauffre, F., Phi, T.L., El Hadri, B., Reynaud, S., 2018. Current opinion: What is a nanoplastic? Environ. Pollut. 235, 1030–1034.

Grimme, S., Ehrlich, S., Goerigk, L., 2011. Effect of the damping function in dispersion corrected density functional theory. J. Comput. Chem. 32, 1456–1465.

Haldar, S., Muralidaran, Y., Míguez, S.I., Mishra, P., 2023. Eco-toxicity of nano-plastics and its implication on human metabolism: Current and future perspective. Sci. Total. Env. 861, 160571.

He, Y., Cheng, X., Gunjal, S.J., Zhang, C., 2024. Advancing pfas sorbent design: Mechanisms, challenges, and perspectives. ACS Mater. Au 4, 108–114.

Hildebrandt, J., Thünemann, A.F., 2023. Aqueous dispersions of polypropylene: toward reference materials for characterizing nanoplastics. Macromol. Rapid Commun. 44, 2200874.

Jeong, C.B., Kang, H.M., Lee, Y.H., Kim, M.S., Lee, J.S., Seo, J.S., Wang, M., Lee, J.S., 2018. Nanoplastic ingestion enhances toxicity of persistent organic pollutants (pops) in the monogonont rotifer brachionus koreanus via multixenobiotic resistance (mxr) disruption. Res. J. Env. Sci. Toxicol. 52, 11411–11418.

Joo, S.H., Liang, Y., Kim, M., Byun, J., Choi, H., 2021. Microplastics with adsorbed contaminants: Mechanisms and treatment. Env. Chall. 3, 100042.

Khaliullin, R.Z., Bell, A.T., Head-Gordon, M., 2008. Analysis of charge transfer effects in molecular complexes based on absolutely localized molecular orbitals. J. Phys. Chem. 128.

Khaliullin, R.Z., Cobar, E.A., Lochan, R.C., Bell, A.T., Head-Gordon, M., 2007. Unravelling the origin of intermolecular interactions using absolutely localized molecular orbitals. J. Phys. Chem. 111, 8753–8765.

Klungness, G., Byrne, R., 2000. Comparative hydrolysis behavior of the rare earths and yttrium: the influence of temperature and ionic strength. Polyhedron 19, 99–107.

Koelmans, A.A., Mohamed Nor, N.H., Hermsen, E., Kooi, M., Mintenig, S.M., De France, J., 2019. Microplastics in freshwaters and drinking water: Critical review and assessment of data quality. Water Res. 155, 410–422.

Kurwadkar, S., Dane, J., Kanel, S.R., Nadagouda, M.N., Cawdrey, R.W., Ambade, B., Struckhoff, G.C., Wilkin, R., 2022. Per-and polyfluoroalkyl substances in water and wastewater: A critical review of their global occurrence and distribution. Sci. Total. Env. 809, 151003.

Lee, W.S., Kim, H., Sim, Y., Kang, T., Jeong, J., 2022. Fluorescent polypropylene nanoplastics for studying uptake, biodistribution, and excretion in zebrafish embryos. ACS Omega 7, 2467–2473.

Leung, S., Cheung, E., Wanninayake, D., Chen, D., Nguyen, N.T., Li, Q., 2023. Physicochemical properties and interactions of perfluoroalkyl substances (pfas)-challenges and opportunities in sensing and remediation. Sci. Total. Env. 905, 166764.

Liu, J., Ma, Y., Zhu, D., Xia, T., Qi, Y., Yao, Y., Guo, X., Ji, R., Chen, W., 2018a. Polystyrene nanoplastics-enhanced contaminant transport: role of irreversible adsorption in glassy polymeric domain. Environ. Sci. Technol. 52, 2677–2685.

Liu, W., Tang, H., Yang, B., Li, C., Chen, Y., Huang, T., 2023a. Molecular level insight into the different interaction intensity between microplastics and aromatic hydrocarbon in pure water and seawater. Sci. Total. Env. 862, 160786.

Liu, W., Tang, H., Yang, B., Li, C., Chen, Y., Huang, T., 2023b. Molecular level insight into the different interaction intensity between microplastics and aromatic hydrocarbon in pure water and seawater. Sci. Total. Env. 862, 160786.

Liu, P., Wu, X., Liu, H., Wang, H., Lu, K., Gao, S., 2020. Desorption of pharmaceuticals from pristine and aged polystyrene microplastics under simulated gastrointestinal conditions. J. Hazard. Mater. 392, 122346.

Liu, Z., Zhang, Y., Wang, B., Cheng, H., Cheng, X., Huang, Z., 2018b. Dft study on al-doped defective graphene towards adsorption of elemental mercury. Appl. Surf. Sci. 427, 547–553.

Liu, G., Zhu, Z., Yang, Y., Sun, Y., Yu, F., Ma, J., 2019. Sorption behavior and mechanism of hydrophilic organic chemicals to virgin and aged microplastics in freshwater and seawater. Environ. Pollut. 246, 26–33.

Llorca, M., Farré, M., 2021. Current insights into potential effects of micro-nanoplastics on human health by in-vitro tests. Front. Toxicol. 3, 752140.

Llorca, M., Schirinzi, G., Martínez, M., Barceló, D., Farré, M., 2018. Adsorption of perfluoroalkyl substances on microplastics under environmental conditions. Environ. Pollut. 235, 680–691.

Lu, T., Chen, F., 2012. Multiwfn: A multifunctional wavefunction analyzer. J. Comput. Chem. 33, 580–592.

Lu, T., Chen, Q., 2020. Van der waals potential: an important complement to molecular electrostatic potential in studying intermolecular interactions. J. Mol. Model. 26, 315.

Lu, T., Chen, Q., 2022. Independent gradient model based on hirshfeld partition: A new method for visual study of interactions in chemical systems. J. Comput. Chem. 43, 539–555.

Mancini, M., Gioia, V., Simonetti, F., Frugis, A., Cinti, S., 2023. Evaluation of pure pfas decrease in controlled settings. ACS Meas. Sci. Au 3, 444–451.

M.D. Hernando, Mezcua, M., A.F.A.D.B, 2006. Environmental risk assessment of pharmaceutical residues in wastewater effluents. Surf. Waters Sediments. Talanta 69, 334–342.

Minervino, A., Belfield, K.D., 2024. Review of recent computational research on the adsorption of pfass with a variety of substrates. Int. J. Mol. Sci. 25, 3445.

Navarathna, C.M., Pray, H., Rodrigo, P.M., Arwenyo, B., McNeely, C., Reynolds, H., Hampton, N., Lape, K., Roman, K., Heath, M., et al., 2023. Microplastics and per-and polyfluoroalkyl substances (pfas) analysis in sea turtles and bottlenose dolphins along mississippi's coast. Analytica 4, 12–26.

Neese, F., 2018. Software update: the orca program system, Version 4. 0. WIREs Comput. Mol. Sci. 8, e1327.

P. Cervantes-Avilás, Piñas, N.C., J.I.G.C.R, 2017. Influence of wastewater type on the impact generated by tio2 nanoparticles on the oxygen uptake rate in activated sludge process. J. Env. Manag. 190, 35–44, journal of environmental management.

Pelegrini, K., Pereira, T.C.B., Maraschin, T.G., Teodoro, L.D.S., Basso, N.R.D.S., De Galland, R.A., Bogo, M.R., 2023. Micro- and nanoplastic toxicity: A review on size, type, source, and test-organism implications. Sci. Total. Env. 878, 162954.

Peng, L., Fu, D., Qi, H., Lan, C.Q., Yu, H., Ge, C., 2020. Micro- and nano-plastics in marine environment: Source, distribution and threats — a review. Sci. Total. Env. 698, 134254.

Perdew, J.P., Burke, K., Ernzerhof, M., 1996. Generalized gradient approximation made simple. Phys. Rev. Lett. 77, 3865–3868.

Pizzini, S., Giubilato, E., Morabito, E., Barbaro, E., Bonetto, A., Calgaro, L., Feltracco, M., Semenzin, E., Vecchiato, M., Zangrando, R., Gambaro, A., Marcomini, A., 2024. Contaminants of emerging concern in water and sediment of the venice lagoon, italy. Environ. Res. 249, 118401.

Plazinski, W., Dziuba, J., Rudzinski, W., 2013. Modeling of sorption kinetics: the pseudo-second order equation and the sorbate intraparticle diffusivity. Adsorption 19, 1055–1064.

Podder, A., Sadmani, A.A., Reinhart, D., Chang, N.B., Goel, R., 2021. Per and polyfluoroalkyl substances (pfas) as a contaminant of emerging concern in surface water: A transboundary review of their occurrences and toxicity effects. J. Hazard. Mater. 419, 126361.

Pontius, F., 2019. Regulation of perfluorooctanoic acid (pfoa) and perfluorooctane sulfonic acid (pfos) in drinking water: A comprehensive review. Water 11.

Qi, L., Qin, W., 2024. Unveiling the fast adsorption and desorption of heavy metals on/off nanoplastics by real-time in-situ potentiometric sensing. Sci. Total. Env. 943, 173789.

Rai, P.K., Sonne, C., Brown, R.J., Younis, S.A., Kim, K.H., 2022. Adsorption of environmental contaminants on micro- and nano-scale plastic polymers and the influence of weathering processes on their adsorptive attributes. J. Hazard. Mater. 427, 127903.

Rayene, K., Imane, D., Abdelaziz, B., Leila, N., Fatiha, M., Abdelkrim, G., Bouzid, G., Ismahan, L., Brahim, H., Rabah, O., 2022. Molecular modeling study of structures, hirschfield surface, nbo, aim, rdg, igm and 1hnmr of thymoquinone/hydroxypropyl-β-cyclodextrin inclusion complex from qm calculations. J. Mol. Struct. 1249, 131565.

Rayne, S., Forest, K., 2009. Perfluoroalkyl sulfonic and carboxylic acids: A critical review of physicochemical properties, levels and patterns in waters and wastewaters, and treatment methods. J Env. Sci. Heal. A 44, 1145–1199.

Ritchie, H., Spooner, F., Roser, M., 2019. Clean water. Our World Data.

Salawu, O.A., Olivares, C.I., Adeleye, A.S., 2024. Adsorption of pfas onto secondary microplastics: A mechanistic study. J. Hazard. Mater. 470, 134185.

Sandoval, M.A., Calzadilla, W., Vidal, J., Brillas, E., Salazar-González, R., 2024. Contaminants of emerging concern: Occurrence, analytical techniques, and removal with electrochemical advanced oxidation processes with special emphasis in latin america. Environ. Pollut. 345, 123397.

Satpathy, K., Mohanty, A., Natesan, U., Prasad, M., Sarkar, S., 2010. Seasonal variation in physicochemical properties of coastal waters of kalpakkam, east coast of india with special emphasis on nutrients. Environ. Monit. Assess. 164, 153–171.

Shao, Y., Gan, Z., Epifanovsky, E., Gilbert, A.T., Wormit, M., Kussmann, J., Lange, A.W., Behn, A., Deng, J., Feng, X., et al., 2015. Advances in molecular quantum chemistry contained in the q-chem 4 program package. Mol. Phys. 113, 184–215.

Sun, N., Shi, H., Li, X., Gao, C., Liu, R., 2023. Combined toxicity of micro/nanoplastics loaded with environmental pollutants to organisms and cells: Role, effects, and mechanism. Environ. Int. 171, 107711.

Tanaka, K., Takahashi, Y., Kuramochi, H., Osako, M., Tanaka, S., Suzuki, G., 2021. Preparation of nanoscale particles of five major polymers as potential standards for the study of nanoplastics. Small 17, 2105781.

Townsend, P.A., 2024. Adsorption in action: Molecular dynamics as a tool to study adsorption at the surface of fine plastic particles in aquatic environments. ACS Omega 9, 5142–5156.

Tseng, L.Y., You, C., Vu, C., Chistolini, M.K., Wang, C.Y., Mast, K., Luo, F., Asvapathanagul, P., Gedalanga, P.B., Eusebi, A.L., Gorbi, S., Pittura, L., Fatone, F., 2022. Adsorption of contaminants of emerging concern (cecs) with varying hydrophobicity on macro- and microplastic polyvinyl chloride, polyethylene, and polystyrene: Kinetics and potential mechanisms. Water 14.

Vareda, J.P., 2023. On validity, physical meaning, mechanism insights and regression of adsorption kinetic models. J. Mol. Liq. 376, 121416.

Wang, F., Shih, K.M., Li, X.Y., 2015. The partition behavior of perfluorooctanesulfonate (pfos) and perfluorooctanesulfonamide (fosa) on microplastics. Chemosphere 119, 841–847.

Wang, Q., Tsui, M.M., Ruan, Y., Lin, H., Zhao, Z., Ku, J.P., Sun, H., Lam, P.K., 2019. Occurrence and distribution of per-and polyfluoroalkyl substances (pfass) in the seawater and sediment of the south china sea coastal region. Chemosphere 231, 468–477.

Wee, S.Y., Aris, A.Z., 2017. Endocrine disrupting compounds in drinking water supply system and human health risk implication. Environ. Int. 106, 207–233.

Wee, S.Y., Aris, A.Z., 2023. Revisiting the forever chemicals, pfoa and pfos exposure in drinking water. NPJ Clean Water 6, 57.

Weigend, F., Ahlrichs, R., 2005. Balanced basis sets of split valence, triple zeta valence and quadruple zeta valence quality for h to rn: Design and assessment of accuracy. Phys. Chem. Chem. Phys. 7, 3297–3305.

Yee, M.S.L., Hii, L.W., Looi, C.K., Lim, W.M., Wong, S.F., Kok, Y.Y., Tan, B.K., Wong, C.Y., Leong, C.O., 2021. Impact of microplastics and nanoplastics on human health. Nanomaterials 11, 496.

Zenobio, J.E., Salawu, O.A., Han, Z., Adeleye, A.S., 2022. Adsorption of per-and polyfluoroalkyl substances (pfas) to containers. J. Hazard. Mater. Adv. 7, 100130.

Zhang, B., Song, X., Zhang, Y., Han, D., Tang, C., Yu, Y., Ma, Y., 2012. Hydrochemical characteristics and water quality assessment of surface water and groundwater in songnen plain, northeast china. Water Res. 46, 2737–2748.

Zhao, X., Gao, P., Zhao, Z., Wu, Y., Sun, H., Liu, C., 2024. Microplastics release from face masks: Characteristics, influential factors, and potential risks. Sci. Total. Env. 921, 171090.